





ARTICLE

Assessment of cracking performance in edge restrained RC walls

Abobakr Elwakeel¹ | Muhammad Shehzad²  | Karim El Khoury¹ |
Robert Vollum¹  | John Forth²  | Bassam Izzuddin¹ | Nikolaos Nikitas² 

¹Department of Civil and Environmental Engineering, Imperial College London, London, UK

²School of Civil Engineering, University of Leeds, Leeds, UK

Correspondence

Robert Vollum, Department of Civil and Environmental Engineering, Imperial College London, London, UK.
Email: r.vollum@imperial.ac.uk

Funding information

Engineering and Physical Sciences Research Council, Grant/Award Numbers: EP/T004142/1, EP/T004185/1

Abstract

Excessive cracking due to restraint of thermal and shrinkage strains is a widespread problem in the concrete construction industry. In design, restraint induced cracking is managed by the provision of reinforcement intended to distribute internal strains in such a way as to control the cracking pattern and limit crack widths. The area of secondary (horizontal) reinforcement required in members such as retaining walls and water tanks is often governed by the need to control early age thermal cracking. This paper presents results from four edge restrained walls tested at Imperial College London and the University of Leeds as part of an Engineering and Physical Sciences Research Council funded project into restraint induced cracking. The paper describes the development of volumetric strain and cracking in the tested walls. The cracking performance is assessed by comparing the restrained strain with the tensile strain capacity of concrete.

KEYWORDS

degree of restraint, early age, edge restraint, imposed strain, thermal strain

1 | BACKGROUND

1.1 | Introduction

Concrete structures undergo early age as well as long-term (LT) volumetric changes due to several actions including early-age thermal (EAT) strains and LT shrinkage strains.¹ If these strains are restrained either internally (by reinforcement or another part of the same cross

section) or externally by adjoining members, stresses develop in the concrete with a magnitude proportional to the restrained strain. This phenomenon can lead to cracking if the stress levels exceed the tensile strength of the concrete.²

Little experimental work has been carried out to investigate cracking in edge restrained members which are the subject of this paper. Stoffers³ examined the influence of reinforcement ratio, wall aspect ratio and presence or absence of wall curvature in 18 tests of reduced scale micro-concrete walls with cross section of $60 \times 375 \text{ mm}^2$. The maximum reinforcement diameter was 3 mm. Kheder et al.⁴ examined the influence of wall aspect ratio. They tested 14 reduced-scale mortar walls

Discussion on this paper must be submitted within two months of the print publication. The discussion will then be published in print, along with the authors' closure, if any, approximately nine months after the print publication.

This is an open access article under the terms of the [Creative Commons Attribution](https://creativecommons.org/licenses/by/4.0/) License, which permits use, distribution and reproduction in any medium, provided the original work is properly cited.

© 2022 The Authors. *Structural Concrete* published by John Wiley & Sons Ltd on behalf of International Federation for Structural Concrete.

with cross section of $100 \times 500 \text{ mm}^2$ reinforced with a central single layer of 8 mm diameter horizontal and vertical bars. Although informative the tests of Stoffers and Kheder et al. are unrepresentative of practical construction due to the use of micro-concretes and small diameter reinforcement. More recently, Micallef⁵ tested a series of edge restrained walls cast onto a kicker connected to a steel beam with shear studs. A drawback with this test arrangement is that substituting the concrete base with a steel beam affects the thermal flow between restrained and restraining elements at the joint level. The only reported experimental work on full-scale walls cast against a concrete base is that of Shehzad⁶ who tested four walls in a pilot study for this project. The walls measured 0.8 m high with aspect ratio of 4.0 and thickness of either 200 or 300 mm and were cast 28 days after the base. In these walls, the ratio of base to wall cross-sectional area was 1.275 for the 200 mm thick walls and 0.85 for the 300 mm thick walls. The tests investigated the effect of varying the ratios of horizontal and vertical reinforcement in the walls. For each wall thickness, the vertical reinforcement in each face comprised either 10 mm diameter bars at 1040 mm centers or 16 mm diameter bars at 150 mm centers. The horizontal reinforcement, in all walls, consisted of 10 mm bars at 180 mm centers in each face. Cracking occurred in both the 0.2 and 0.3 m thick walls with vertical 16 mm bars at 150 mm centers in each face. Shehzad⁶ measured surface strains between points in a regular orthogonal grid of demec points. The initial demec readings within the central region of the wall were taken within 1 h of stripping the formwork which was typically removed 20 h after casting when the maximum wall temperature was close to its peak. The crack inducing strain was obtained by subtracting the measured surface strain from the free strain which was calculated as the sum of the thermal and shrinkage strains occurring subsequent to the initial set of demec readings. The resulting crack inducing strains were compared with the tensile strain capacity of the concrete which was determined using CIRIA report C660.⁷ Cracking is predicted to be likely by C660⁷ if the crack inducing strain exceeds the tensile strain capacity. The method correctly predicted cracking to only occur in the walls with vertical reinforcement consisting of 16 mm bars at 150 mm centers. These tests highlight the influence of vertical reinforcement on the degree of restraint as well as the importance of heat exchange between the base and the wall.

Design provisions pertinent to crack control in edge restrained members are given in several codes^{8,9} as well as CIRIA Report C766¹⁰ which is used extensively in the UK. However, these provisions (particularly those

pertaining to edge restraint) are empirical in nature and, somewhat contradictorily, are reported to result in both over-conservative designs¹¹ as well as excessive cracking.^{1,12,13} The occurrence of excessive cracking despite following current guidance in codes of practice requires further detailed study.

This paper presents the results of four tests on edge restrained walls carried out at Imperial College London (ICL; walls ICL-1 and ICL-2) and University of Leeds (UoL; walls UoL-1 and UoL-2). The tests investigated the influence on crack inducing strain of wall aspect ratio, ratio of wall to base cross-sectional area and concrete mix design.

1.2 | Test details and set up

The first two tests (ICL-1 and UoL-1) were on geometrically identical reinforced concrete walls measuring 5.2 m long, 1.3 m high, and 250 mm thick as shown in Figure 1. The walls were cast onto 6 m long, 0.9 m wide, and 300 mm thick base slabs. The aspect ratio of these walls was chosen to equal 4.0 which is considered representative of practice based on the experience and comments from industrial collaborators and steering committee members. The adopted wall dimensions are the largest that can readily be handled in the Large Structures Laboratory at ICL. The specimen dimensions were obtained by scaling up those of the four walls tested by Shehzad⁶ in a pilot study at UoL. In tests ICL-1 and UoL-1, the ratio of base to wall cross-sectional area was 0.83 which is similar to the 300 mm thick walls tested in the pilot study of Shehzad.⁶ Walls ICL-1 and UoL-1 did not crack. Consequently, the ratio of base to wall cross-sectional area was increased in tests ICL-2 and UoL-2. At ICL this was done by reducing the wall height to 1 m over a length of 3.8 m centered on the wall centreline as shown in Figure 2. The height of the end 0.7 m lengths of the wall was maintained at 1.3 m to enable the top of the wall to be externally loaded through a strut and hydraulic jack bearing on the upstands. Two 250 mm square openings were also cast into the bottom of the wall adjacent to the 0.7 m wide upstands to enable the wall to be externally loaded in tension via a pair of struts and hydraulic jacks bearing onto cross beams threaded through each opening. The ratio of base to wall cross-section area for wall ICL-2 was 1.05. At UoL, the height of wall UoL-2 was also reduced to 1.0 m, but the aspect ratio was maintained at 4.0 while increasing the base dimensions to 1 m wide by 400 mm thick giving a ratio of base to wall cross-sectional area of 1.6. Detailed dimensions and steel reinforcement details are presented for walls ICL-1, UoL-1, and ICL-2 in Table 1 and in Figures 1 and 2. The

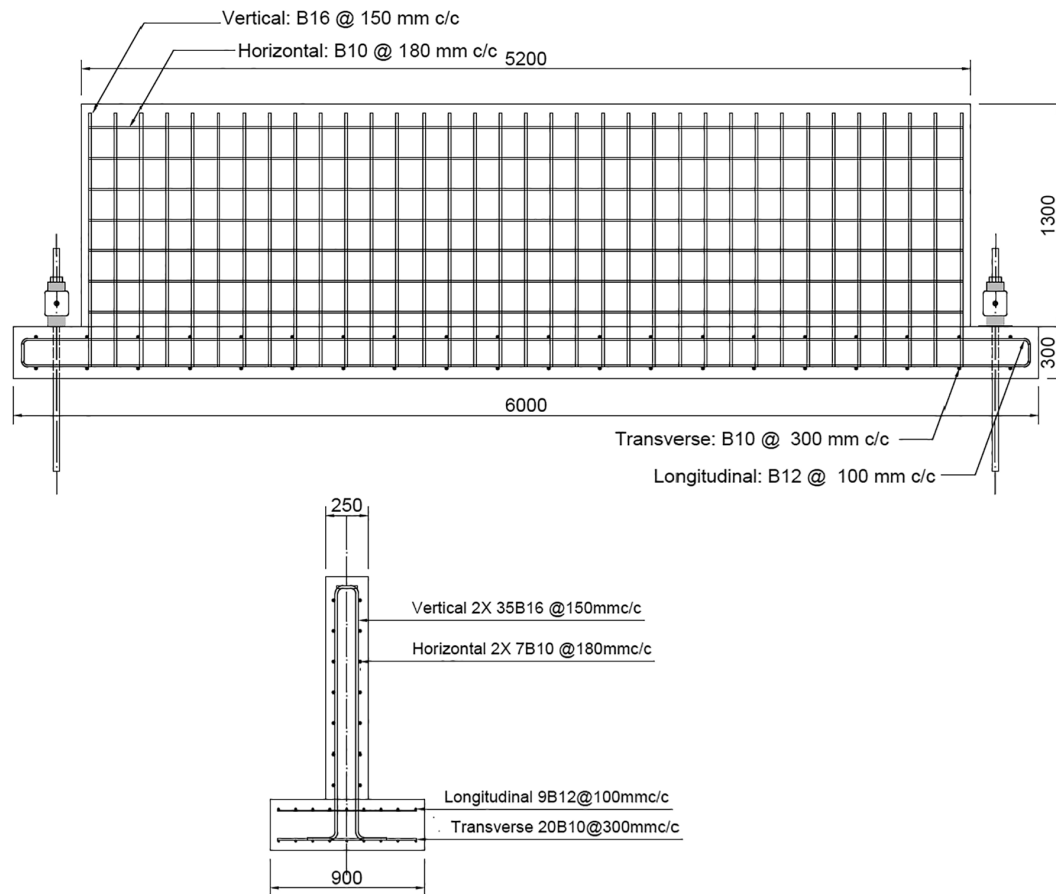


FIGURE 1 Geometry and reinforcement of walls ICL-1 and UoL-1. ICL, Imperial College London; UoL, University of Leeds

reinforcement bar diameters and spacings were identical in walls UoL-1 and UoL-2.

The base slab of all walls was cast at least 28 days prior to casting of the wall as indicated in Table 3. The top of the base was roughened manually immediately after casting to obtain a rough interface between the wall and slab. At ICL, localized mechanical scabbling was also carried out to roughen the surface of the hardened concrete and break out any loose concrete. Longitudinal strain was monitored in the base from the time the side shuttering was removed at ICL and end of curing at UoL. The walls were monitored for a minimum period of 12 weeks from casting at ICL and 8 weeks at UoL.

The strain distribution in edge restrained walls depends significantly on whether the wall is constrained to remain straight or is free to curl under differential strain between the wall and base.³ Upwards curling of the wall ends was prevented by tying the ends of the base down to the laboratory strong floor with a pair of bolts as shown in Figure 1. The bolts were prestressed to a load of 100kN prior to casting the wall. The prestress was monitored throughout each test using load cells and was found to remain almost constant throughout the tests.

1.3 | Materials and procedures

Ready-mix concrete procured from the same vendor was used at both institutions. Limestone coarse aggregate was used throughout since this is the only aggregate type commonly available in Leeds. The concrete mix design was varied between the walls as shown in Table 2. Mix ICL-M1, which was used in wall ICL-1, had the same composition as the concrete mix used in the pilot study of Shehzad.⁶ The initial intention was to use this mix for all the walls but, in the event, wall ICL-1 which was cast in advance of UoL-1 did not crack. Consequently, the concrete mix design was revised for wall UoL-1 by increasing both the percentage of fines and the water to cement ratio. This was done to reduce the concrete strength, and hence cracking strain, and to increase the free shrinkage strain. In specimens ICL-1 and UoL-1, the same concrete mix design was used for both the wall and the base. The base of ICL-2 was cast at the same time as wall ICL-1 using concrete from the same lorry. Nominally the same concrete mix, but adjusted for local variations in aggregate, was used in wall ICL-2 as UoL-1. Since wall UoL-1 did not crack, the percentage of fines

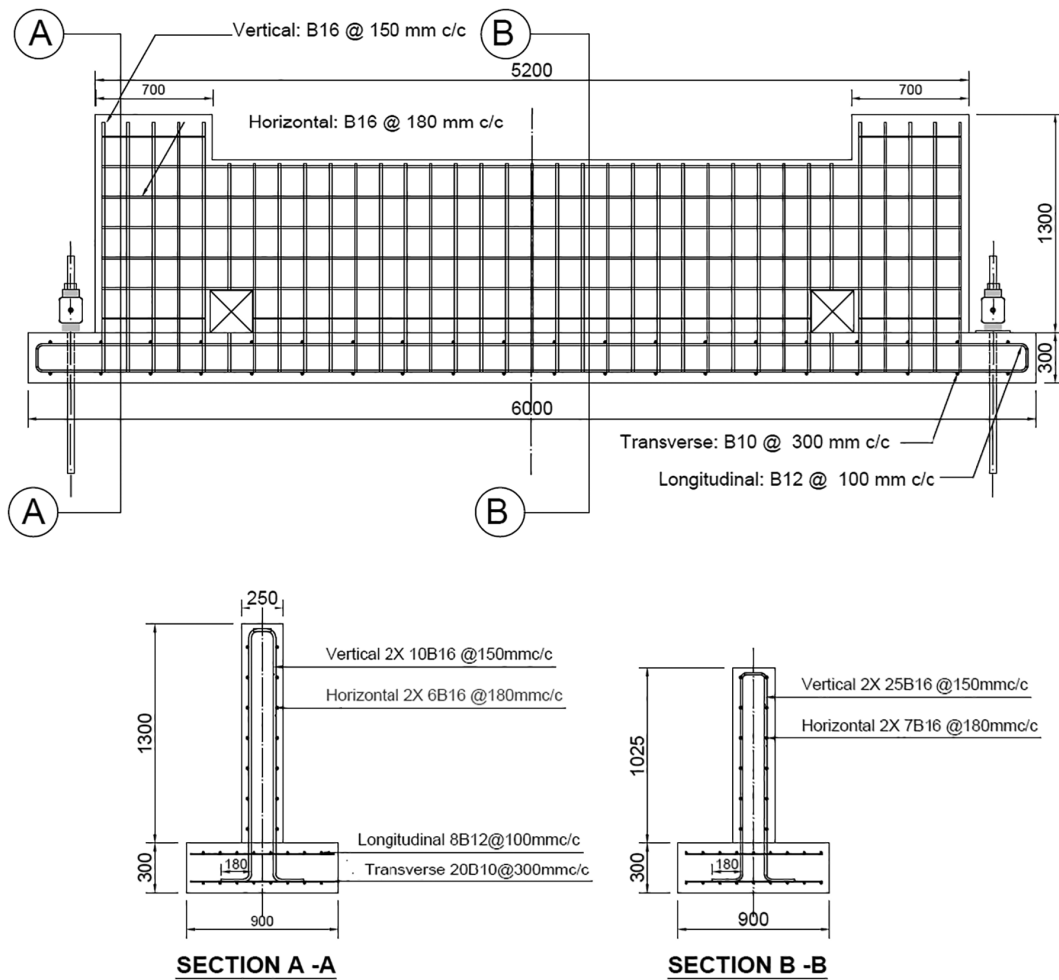


FIGURE 2 Geometry and reinforcement of wall ICL-2. ICL, Imperial College London

and cement content were reduced in the wall of UoL-2, while maintaining a high water to cement ratio, in order to reduce the cracking strain while reducing concrete creep and maintaining a high shrinkage strain. The detailed compositions of the concrete mixes used, and their allocation are provided in Table 2.

Mean values of the concrete compressive strength (cube [f_{cum}] and cylinder [f_{cm}]), split cylinder concrete tensile strength (f_{ctm}) and concrete elastic modulus (E_m) were determined for each base and wall. The tests were carried out in accordance with the relevant part of BS EN 12390.^{14,15,16} All the cube tests were carried out on 100 mm cubes. The elastic modulus and compressive cylinder strengths were obtained from 100 mm diameter by 200 mm long cylinders at ICL and 150 mm diameter by 300 mm long cylinders at UoL. The split cylinder tensile strengths were determined from cylinders measuring 150 mm diameter by 300 mm long. The resulting 28-day material properties are listed in Table 3 for each base and wall. The mean strengths listed in Table 3 are the average of the results of three tests on specimens cured in water

at 20°C. With the exception of wall ICL-2, concrete strengths were not measured beyond 28 days. In wall ICL-2 the cube strength at 132 days was 53.85 MPa. Shrinkage development in concrete cylinders and prisms was measured throughout the duration of tests and was compared to the shrinkage profiles obtained using design codes as described in Section 2.2.

At ICL, a temperature matched curing tank was used to obtain the early age concrete compressive strength development for wall ICL-2. A schematic drawing of the temperature-matched curing process is shown in Figure 3. The match cured water tank temperature was programmed to track the peak temperature of wall ICL-2 following casting. The early age strengths of the temperature of the match cured cubes were significantly greater than those of cubes cured at 20°C as shown in Figure 4 with relative increases in strength of 71%, 34%, and 15% at 1, 2, and 3 days, respectively. The strengths were similar for both curing conditions at 28 days.

Details of the formwork and insulation used at each institution are shown in Figure 5. At ICL, the formwork

TABLE 1 Geometry and reinforcement details of the walls and bases

Wall	ICL-1	ICL-2	UOL-1	UOL-2
Base dimensions				
Length – L_b (mm)	6000	6000	6000	5400
Width – W_b (mm)	300	300	300	400
Thickness – T_b (mm)	900	900	900	1000
Wall dimensions				
Length – L_w (mm)	5200	5200	5200	4000
Height – H_w (mm)	1300	1025	1300	1000
Thickness – T_w (mm)	250	250	250	250
L_w/h_w	4	5.1	4	4
A_{base}/A_{wall}	0.83	1.05	0.83	1.60
Base reinforcement				
Longitudinal				
Dia(mm)	12	12	12	12
Spacing (mm)	100	100	100	100
Transverse				
Dia(mm)	10	10	8	8
Spacing (mm)	300	300	200	200
Wall reinforcement				
Vertical				
Dia(mm)	16	16	16	16
Spacing (mm)	150	150	150	150
ρ_v (%)	1.07	1.07	1.07	1.07
Horizontal				
Dia(mm)	10	16	10	10
Cover (mm)	25	25	30	30
Spacing (mm)	180	180	180	180
ρ_h (%)	0.35	0.89	0.34	0.38

TABLE 2 Mix design and allocation

Wall	ICL-M1	ICL-M2	UoL-M1	UoL-M2
Cement content (kg/m ³)	385	410	410	280
20 mm, Limestone (kg/m ³)	819	392	381	475
10 mm, Limestone (kg/m ³)	545	261	254	316
Sand (kg/m ³)	730	973	945	985
w/c ratio	0.45	0.60	0.60	0.70
Water content (kg/m ³)	175	245	245	196
Location	ICL-Wall1	ICL-Wall2	UoL-Wall1	UoL-Wall2
	ICL-Base1		UoL-Base1	
	ICL-Base2		UoL-Base2	

consisted of 19 mm sheets of plywood spanning between 145 by 70 mm² horizontal timber joists spaced at 250 mm centers. To maximize the temperature rise, insulation

consisting of 50 mm thick polyisocyanurate (PIR) sheets having thermal conductivity of 0.022 W/mK were placed between the joists, at the ends of the wall and on top of

	ICL 1	ICL 2	UoL 1	UoL 2
Wall				
f_{cm} (28 day) MPa	51.8	42.6	51.8	28.6
f_{ctm} (28 day) MPa	3.4	3.22	3.77	1.93
E_{cm} (28 day) GPa	35.7	30.9	31.4	29.9
Slump (mm)	36	220	155	60
Base				
f_{cm} (28 day) MPa	45.6	51.8	43.2	45.5
f_{ctm} (28 day) MPa	3.84	3.4	4.38	3.96
Age at casting the wall (days)	48	184	28	28

TABLE 3 Concrete mixes properties

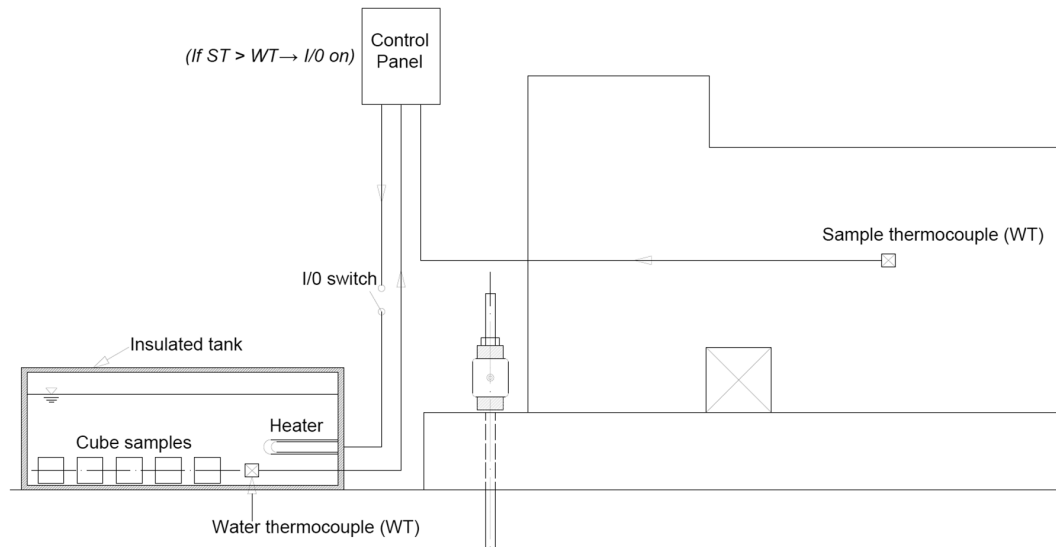


FIGURE 3 Schematic drawing of the temperature-matched curing process

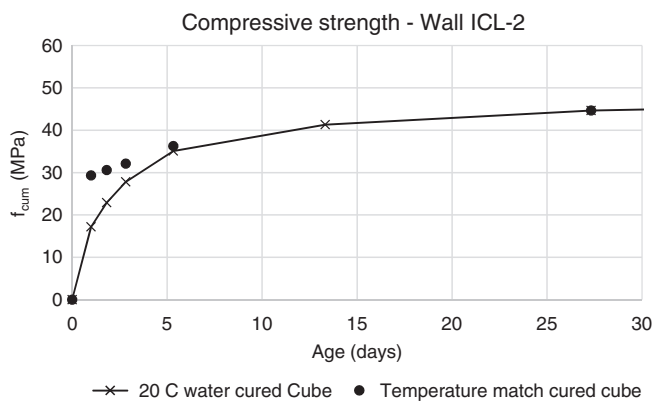


FIGURE 4 Temperature matched cube strengths for wall ICL-2. ICL, Imperial College London

the freshly cast concrete. Modular formwork with 10 mm thickness made of techno-polymers having a thermal conductivity of 0.25 W/mK was used at UoL. No

additional insulation was used for wall UoL-1 but for wall UoL-2, the modular formwork was insulated externally with 100 mm of sheep wool having thermal conductivity of 0.039 W/mK.

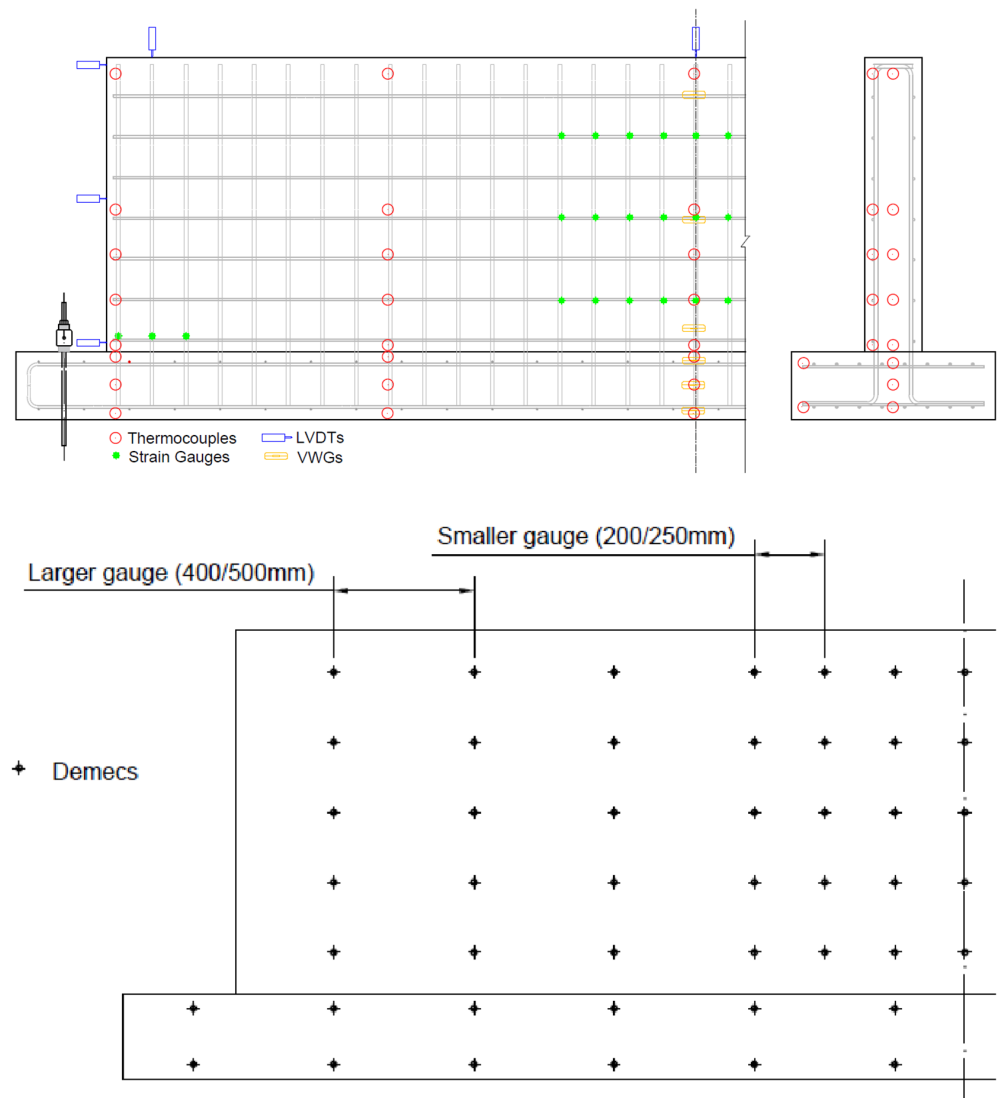
1.4 | Instrumentation

Volumetric and surface strains occurring in the base and walls were monitored with demountable mechanical gauge (demec) grids, digital image correlation (DIC) and vibrating wire gauges (VWGs; see Figure 6). Only the demec strains are reported in this paper. The resolution of the digital demec gauges used was 0.0008 mm which corresponds, for example, to a strain of 4 μ s over a gauge length of 200 mm. The accuracy of the demec readings is operator dependent but typically within 10 μ s. Selected reinforcement strains were measured with surface mounted electrical resistance strain gauges. At ICL, the

FIGURE 5 Formwork used at (a) ICL and (b) UoL. ICL, Imperial College London; UoL, University of Leeds



FIGURE 6 Details of instrumentation, sensors, and demec grids used in the tests



demec points along the edge of the base were fixed on the same day as the side shuttering was removed. At UoL, the base slabs were cured under wet hessian for 14 days prior to fixing the demec points. The grids of points on the wall were fixed as rapidly as possible to minimize loss of temperature prior to the first set of demec readings. The demec points were set out from the center of the wall, on one face only, with initial readings taken within the central region of the wall prior to completion of the grid at the wall ends. Strains in the other wall face were monitored at ICL using a DIC system. The VWGs, which are not reported here, give insight into the development of volumetric strain in the concrete during both the heating and cooling phases.

The concrete temperature was monitored using K-type thermocouples installed at locations based on thermo-mechanical nonlinear finite element analysis. Additionally, linear variable displacement transducer (LVDTs) were installed to monitor base uplift and overall deformation. A typical instrumentation layout is shown in Figure 6, however, the exact number of temperature sensors was varied slightly between tests to establish localized variations in temperature.

To estimate the free shrinkage of each mix, concrete prisms and cylinders were cast from the same concrete mix as the wall specimens and cured in air alongside the

walls. Shrinkage strains were monitored in these specimens using a demec gauge. At ICL, a plain concrete panel measuring 1.0 m by 1.0 m by 250 mm was cast at the same time as wall ICL-2 (see Figure 7). The formwork for the panel consisted of 19 mm plywood insulated with 50 mm thick PIR sheets like the ICL walls. The early age temperature rise of the panel was monitored with thermocouples which showed the early age temperature rise of the trial panel to be similar to that of the wall as intended. Two VWGs were placed horizontally and vertically at the center of the panel. Surface strains were measured from around 1 h after removal of formwork with a grid of 16 demec points positioned at horizontal and vertical spacings of 250 mm (see Figure 7b). These strains were used in the estimation of free strain in wall ICL-2.

2 | RESULTS AND DISCUSSION

Following casting, the temperature of the concrete in the walls increased due to the heat of hydration of the cement. The temperature rise depends principally on the cement content, and type, and the thermal resistance of the formwork although it is influenced by other factors such as aggregate type. Heat was lost from the wall

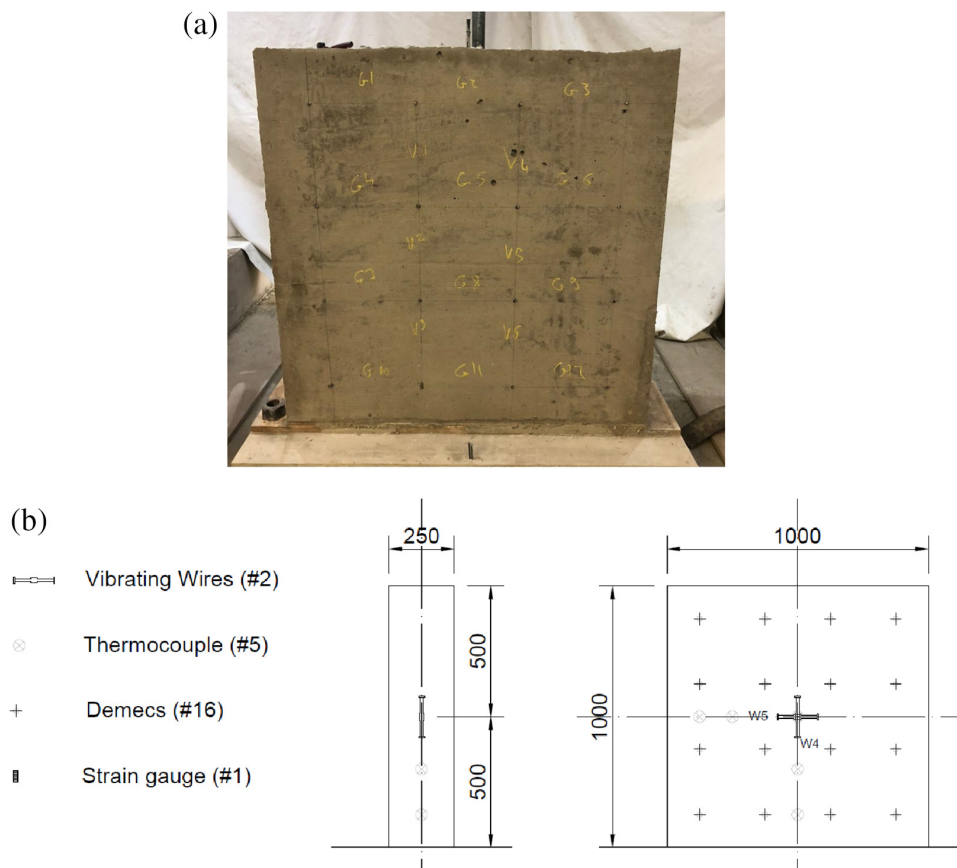


FIGURE 7 Instrumentation of the trial panel of wall ICL-2. ICL, Imperial College London

through the base giving rise to a temperature gradient over the height of the wall with the temperature least at the bottom of the wall. The formwork was removed from the walls between 18 and 21 h from casting when the temperature was close to its peak value. The concrete in the walls expanded during the heating phase, while the concrete was hardening. During this phase the expansion of the concrete in the wall is restrained by the base causing the concrete in the wall to go into compression and the base into tension. Subsequently, the wall contracts as it cools following removal of the formwork. The contraction of the wall during cooling and subsequent differential shrinkage with respect to the base causes tensile stress to develop in the wall. Guidance on estimating the likelihood of cracking in edge restrained walls is given in CIRIA Reports C660⁷ and C766.¹⁰ In

this approach, which is assessed in this paper, cracking is assumed to occur if the crack inducing strain exceeds the tensile strain capacity of the concrete. The crack inducing strain is assumed to equal the difference between the total strain and the free strain that develops due to the temperature drop from peak and concrete shrinkage. Reports C660⁷ and C766¹⁰ give empirical expressions for the tensile strain capacity which allow for the influence of the initial compressive strain induced during the heating phase as well as creep. An alternative to the CIRIA^{7,10} approach is to calculate the tensile stress induced by contraction from the point the stress changes sign from compression to tension. This approach is adopted in Annex D of prEN 1992-1¹⁷ which assumes that 90% of the drop in temperature from peak contributes to the development of tensile stress. The

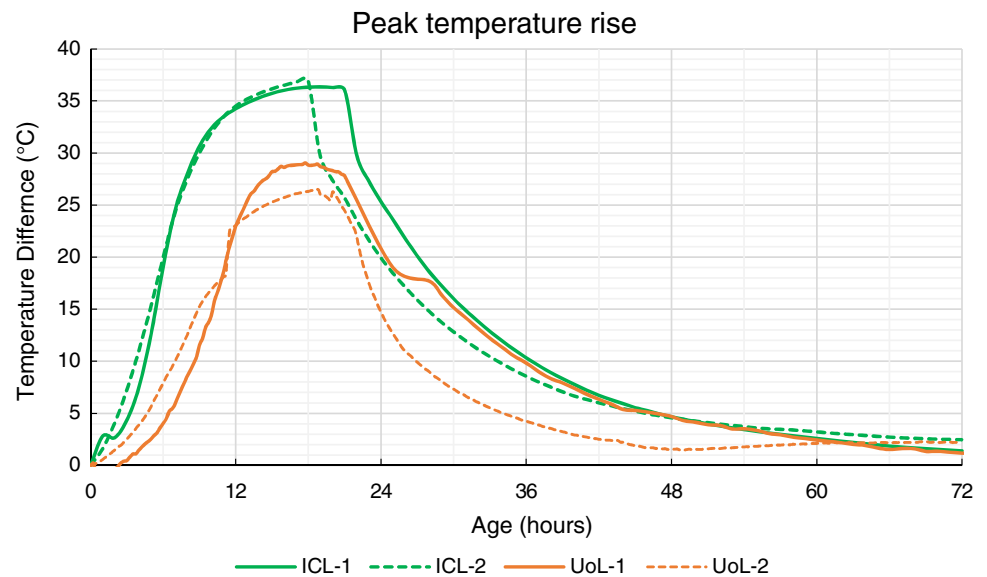


FIGURE 8 Peak temperature profile of the tested walls

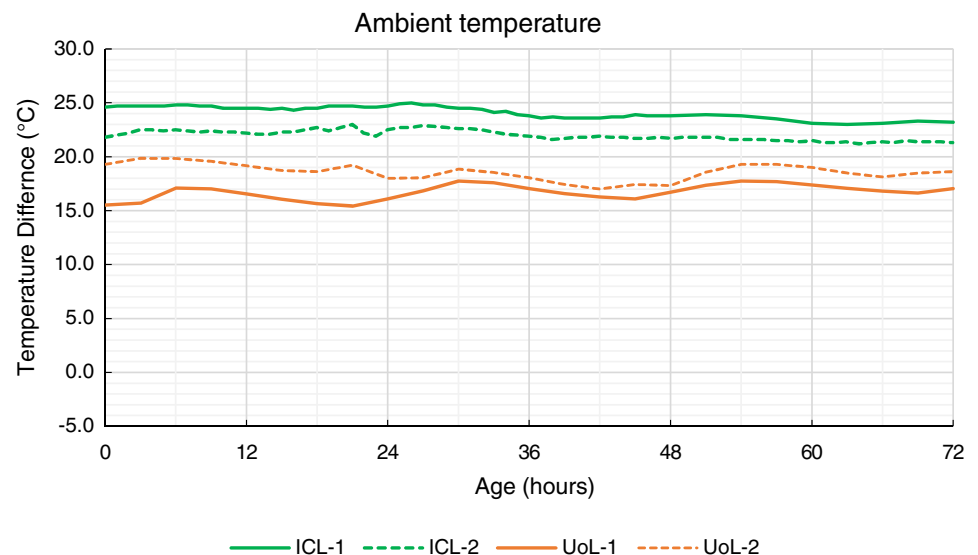


FIGURE 9 Ambient temperature profiles of the tested walls

Annex D approach is not very different to that adopted in this paper due to the temperature drop from peak at first demec reading being around 10% of the drop from peak to ambient.

The next sections present the experimental results and describe the methodology used to estimate the degree of restraint and cracking performance.

2.1 | Temperature profiles and estimation of thermal strains

At ICL, the peak wall temperature coincided with removal of the formwork which was done sequentially with formwork on the demec grid side removed first and formwork on the other side removed immediately after. At UoL, the formwork panels of the modular system were removed sequentially leading to a less sudden drop of temperature following formwork removal. The peak temperature rise, relative to the initial concrete temperature, and subsequent temperature drop over the first 72 h are shown for each wall in Figure 8.

The variation in peak temperatures evident in Figure 8 is a function of the different formwork used at ICL and UoL as well as the different concrete mix designs. The supplementary sheep wool insulation used in test UoL-2 is seen to have largely compensated for the reduced heat of hydration of mix UoL-M2 relative to UoL-M1 resulting from the reduction in cement content from 410 to 280 kg/m³ (see Table 2). Figure 9 shows the ambient temperature profiles in the laboratory over the first 72 h following casting of the walls. Figures 10 and 11 depict the variation in temperature with relative height (h/H , where h is height measured from the top of the base and H is the wall height) at the thermocouples

positioned at the center and toward the ends the walls (see Figure 6) respectively. The temperature rises at the thermocouples positioned at approximately one fourth of the wall length from the wall ends were similar to those at corresponding positions at the wall center. The temperature rise was lowest toward the bottom of the walls and increased gradually along the wall height. The maximum temperature rise occurred between mid-height and the top of walls. This variation in temperature rise is attributable to the exchange of heat between the wall and the base slab as well as to the surrounding environment.

2.2 | Estimation of free strain

The free strain, which equals the sum of the thermal and shrinkage strains, varies over the wall height and length due to the temperature variation evident in Figures 9 and 10. The wall temperature was estimated by linearly interpolating between the temperatures measured at the thermocouples (see Figure 6). Unless more accurate information is available, EC2¹⁸ and EC2 Part 3⁸ state that the coefficient of thermal expansion (CTE) of concrete may be taken as 10 $\mu\epsilon/^\circ\text{C}$. In reality, as acknowledged in EC2 Part 3, the CTE of concrete varies depending on the type of coarse aggregate used with suggested¹⁰ values ranging between around 9 $\mu\epsilon/^\circ\text{C}$ for limestone aggregate and 13 $\mu\epsilon/^\circ\text{C}$ for gravel aggregate. The CTE was estimated to be 8.5 $\mu\epsilon/^\circ\text{C}$ for mix ICL-M2 from demec strain measurements in a concrete cylinder with an embedded thermocouple as well as analysis of early age strain in the trial panel. The cylinder was heated in a water bath from room temperature to 60 $^\circ\text{C}$ in increments of around 15 $^\circ\text{C}$. The CTE was determined from strain measurements taken at each temperature interval. The obtained value of 8.5 $\mu\epsilon/^\circ\text{C}$ is similar to that of 9.0 $\mu\epsilon/^\circ\text{C}$ given by¹⁰ for

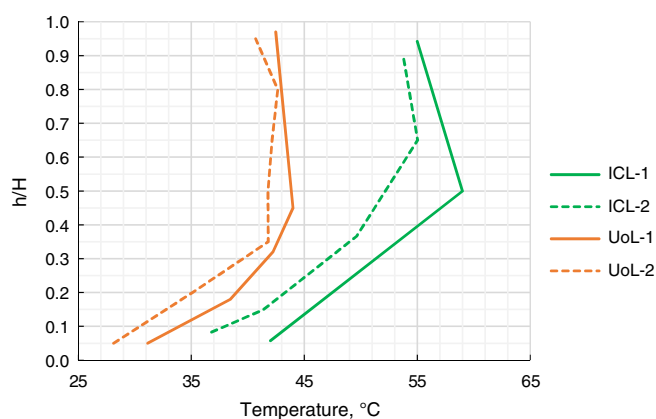


FIGURE 10 Peak temperature variation along height—middle of the walls

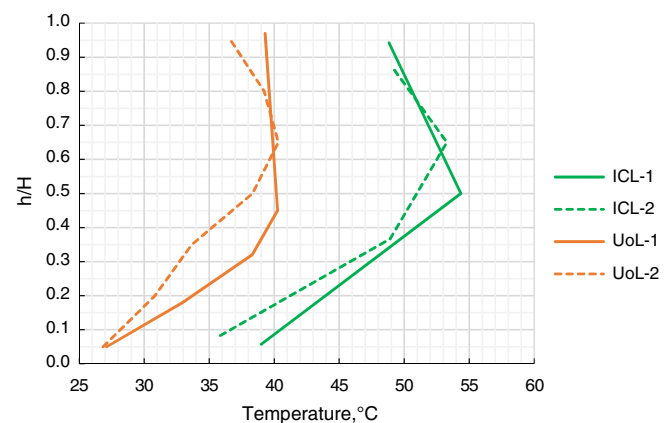


FIGURE 11 Peak temperature variation along height—end of the walls

concrete with limestone aggregate. A CTE of $8.5 \mu\epsilon/^\circ\text{C}$ was also used for wall ICL-1 based on early age temperature adjusted VWG strains measured in its base slab. At UoL, a CTE of $10 \mu\epsilon/^\circ\text{C}$ was adopted.

To estimate shrinkage strains, concrete prisms ($75 \times 75 \times 200 \text{ mm}$) and cylinders (100 mm diameter and 200 mm long) were cast from each batch of concrete and cured in air alongside the tested walls. Strains were measured between pairs of demec points installed on opposite faces of specimens. The measured shrinkage strains were compared with shrinkage calculated using MC2010⁹ and EC2¹⁸ in terms of the measured concrete strength and relative humidity during the tests. The results are presented in Figure 12 which shows that the measured shrinkage strains compare well with the EC2 predictions for concrete mixes ICL-M1, UoL-M1, and UoL-M2. The shrinkage of mix ICL-M2 was significantly greater than predicted even though the mix was nominally similar to UoL-1. A possible explanation for this lies in the slumps which were 220 mm for ICL-M2 compared with 155 mm for UoL-M1. The higher shrinkage of mix ICL-M2 was expected due to its high cement content of

410 kg/m^3 , high w/c ratio of 0.6 and high proportion of fine aggregate. Although these parameters are reported to increase concrete shrinkage,¹⁹ they are not explicitly accounted for in the shrinkage estimation of either EC2 or MC2010. The measured shrinkage strain was also found to be greater than predicted in the trial panel cast alongside wall ICL-2 as shown in Figure 13 where thermal strains and ambient temperature variation strains were subtracted from the total measured strains to obtain shrinkage strains.

Due to the good comparison between measured and calculated strain in the control specimens, free shrinkage strains were estimated in walls ICL-1, UoL-1, and UoL-2 using EC2. This finding is consistent with the findings of Gribniak et al.²⁰ who carried out comparative statistical analysis to assess the accuracy of several well-known shrinkage prediction models (EC2, ACI 209,²¹ CNIIS²² [Russia], Bazant & Baweja's²³ [B3], and Gardner & Lockman's²⁴ [GL 2000]). Their database consisted of 22 experimental programs comprising 351 specimens and 7391 measurement points. EC2 was found²⁰ to be the most accurate shrinkage prediction technique for the

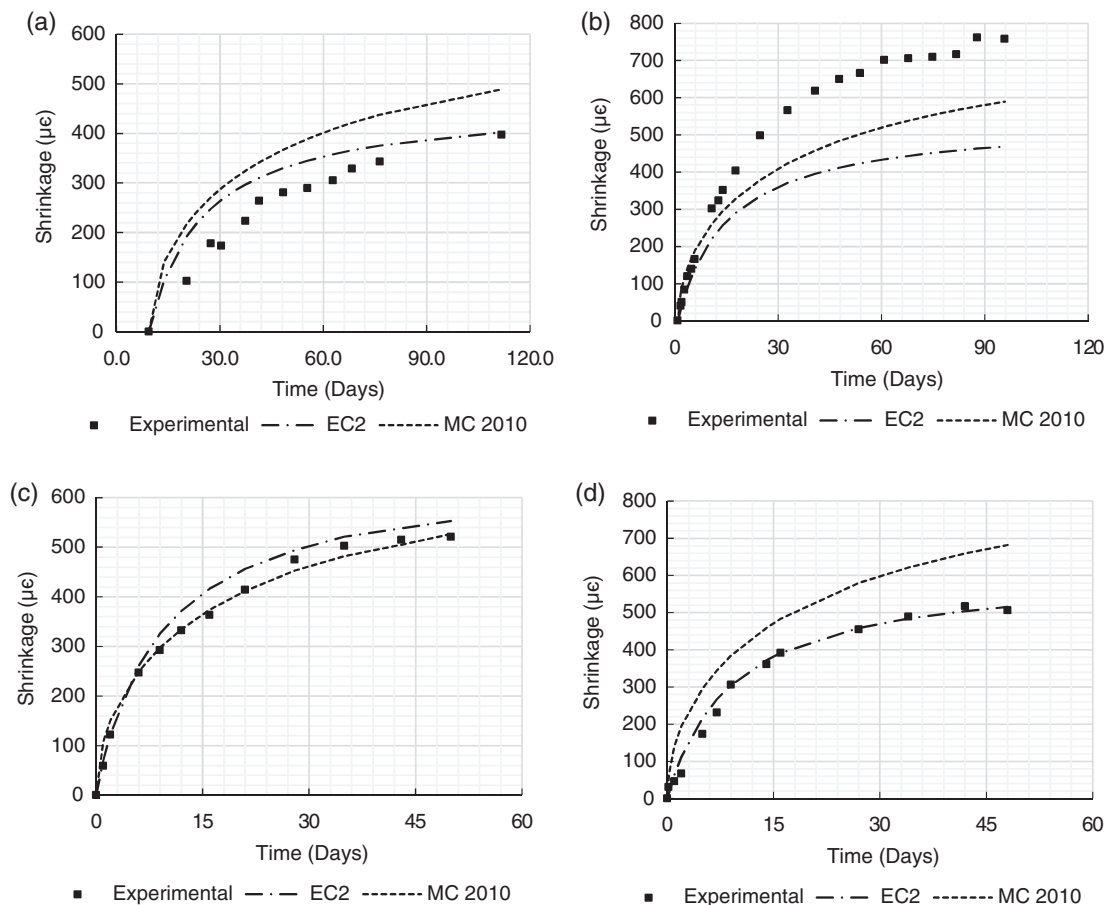


FIGURE 12 Comparison of shrinkage strains in concrete specimens with design codes for walls (a) ICL-1, (b) ICL-2, (c) UoL-1, and (d) UoL-2. ICL, Imperial College London; UoL, University of Leeds

time interval up to 90 days. For wall ICL-2, the shrinkage strain in the wall was taken as that measured in the trial panel. The total free strain (ϵ_{free}) was calculated as:

$$\epsilon_{free} = \epsilon_{sh} + \alpha_c \Delta T \quad (1)$$

in which ϵ_{sh} is the free shrinkage strain, α_c is the CTE, and ΔT is the drop in temperature in the wall from the peak temperature which occurred at or around the time of striking.

2.3 | Variation of concrete surface strain with time

For measurement of surface strain, the tested walls were divided into central and end zones. Smaller demec gauge lengths were used in the middle part of the wall while larger gauge lengths were used at the ends of the walls. At UoL, demec gauge lengths of 400 and 200 mm were used while at ICL gauge lengths of 250 and 500 mm were used. This measurement layout was chosen to save time installing the demec grids given the importance of

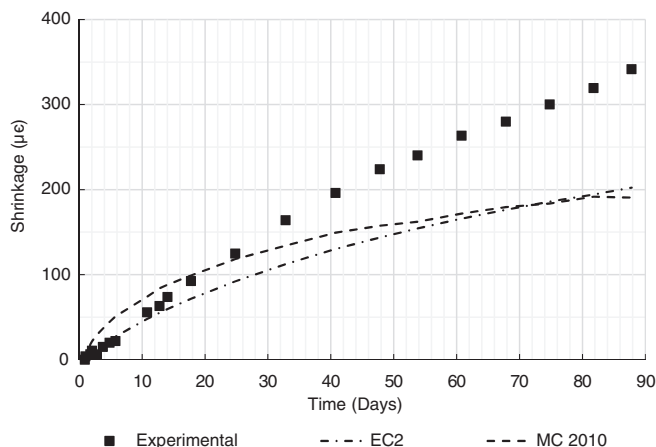


FIGURE 13 Shrinkage strains measured in trial panel of wall ICL-2. ICL, Imperial College London

capturing the EAT strains. Moreover, it has been reported that, in an edge restrained wall, the risk of cracking is more in the central parts of the wall as compared to the ends.^{2,10} The reported surface strains are measured relative to the first set of demec readings after the demec grid was installed. Necessarily, there was a delay as noted in Table 4 between removing the side shuttering to the wall and the taking of a complete set of initial demec points. For each of the zones specified for strain measurement, the average of measured surface strains was calculated and plotted over the relative wall height (h/H) at frequent time intervals as shown in Figure 14 which also shows the estimated free strain corresponding to the final strain profile for all walls. In the legends to Figures 14, 16, and 17 the symbols “d” and “w” depict the time in days and weeks respectively from casting the wall. The time difference in hours, and corresponding average drop in temperature, between removal of the formwork and the reference set of demec readings is given in Table 4 for the middle and end regions of each wall.

The restraining action of the base slab is clearly indicated by the differences between the final free strain and final measured strain indicated in Figure 14. The free strain reduces toward the base of the wall due to the temperature variation shown in Figures 10 and 11 which results from heat being lost to the base. Figure 15 depicts the development of surface strain with time in each wall during the monitoring period at the top, mid-height, and bottom levels of the walls. A sharp increase in the surface strains at all levels can be noticed during the early age (first 3 days) primarily due to thermal contraction, after which strains increase more gradually due to shrinkage. The initial increase in strain with time is most rapid for the ICL walls due to their greater temperature drop from peak to ambient.

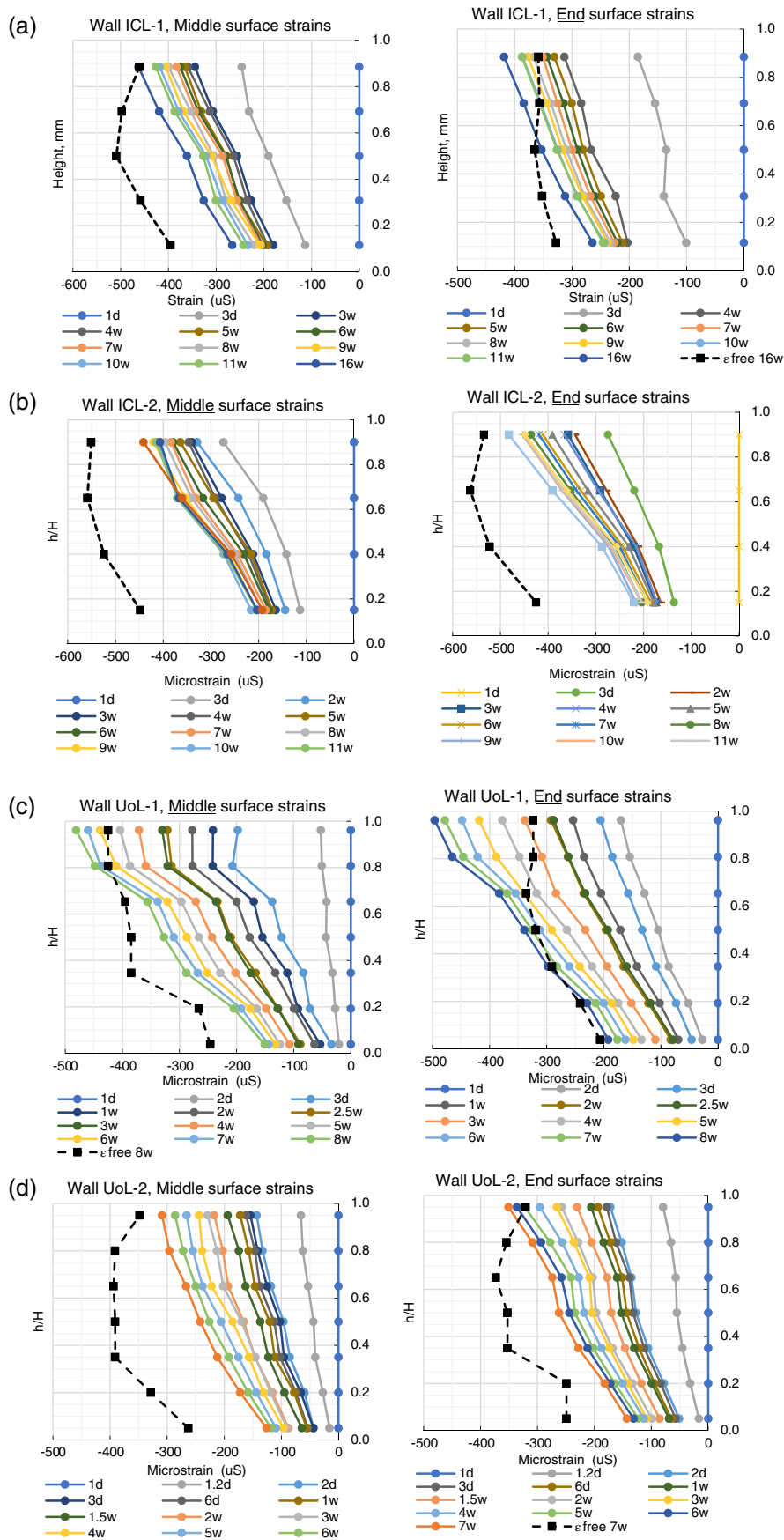
2.4 | Degree of restraint and restraint profiles

The degree of restraint imposed on the wall is conveniently expressed in terms of the restraint factor which

TABLE 4 Time from striking to first demec reading and corresponding average drop in temperature

Wall	End region		Middle region	
	Time for reference reading (h)	Maximum temperature drops from peak (°C)	Time for reference reading (h)	Maximum temperature drops from peak (°C)
ICL-1	6	21	1	2.2
ICL-2	0.75	3.91	0.75	4.66
UoL-1	3.5	5	1.5	2.2
UoL-2	2	2.3	1	1.7

FIGURE 14 Variation with time of the measured surface strains along height of tested walls (a) ICL-1, (b) ICL-2 (c) UOL-1, and (d) UOL-2. ICL, Imperial College London; UoL, University of Leeds



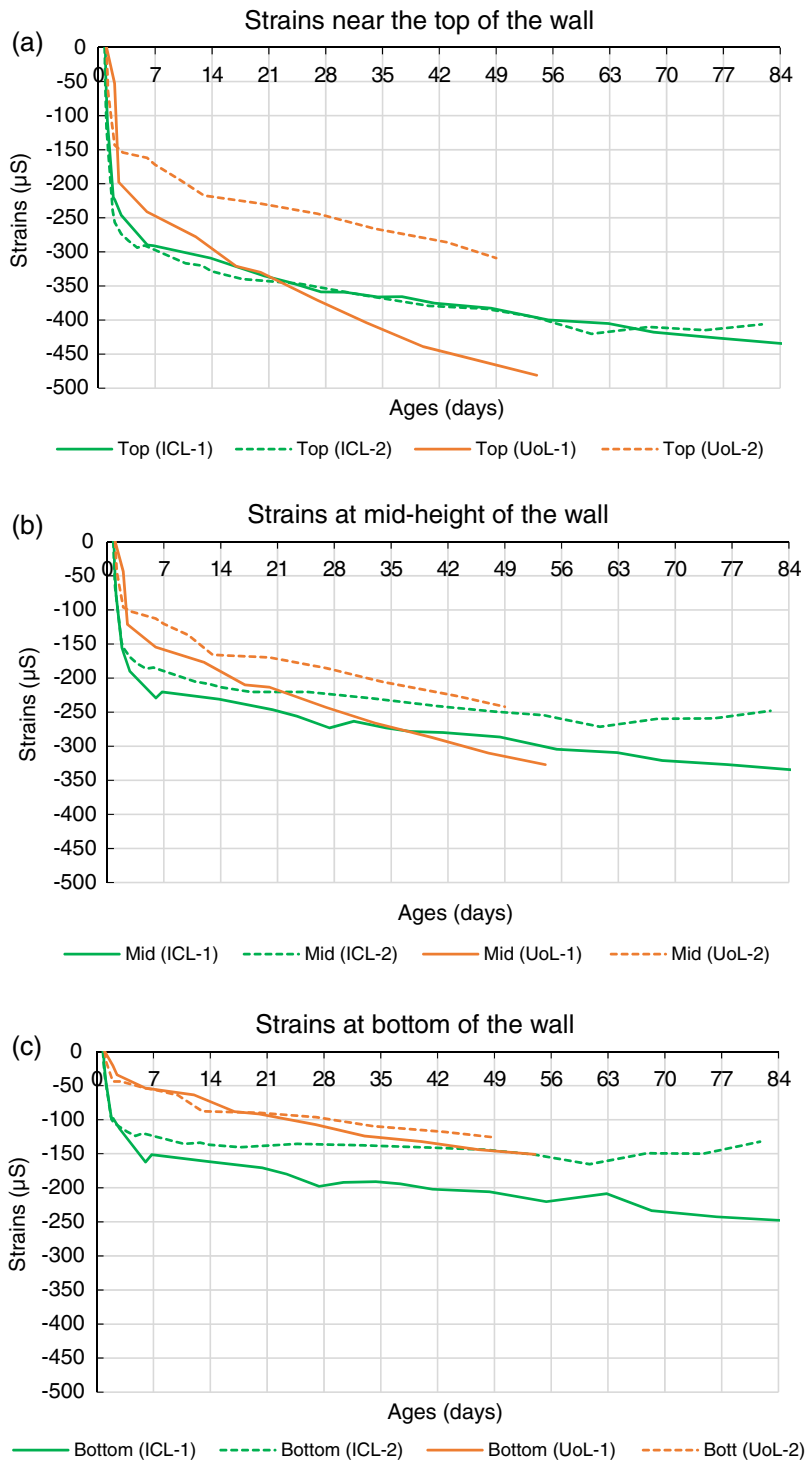


FIGURE 15 Development of surface strains with time in the wall tests

equals the ratio of the restrained strain to the free strain. The restrained strain is given by the difference between the measured surface strain and the corresponding free strain calculated with Equation 1 using the same reference time for both measured and calculated strain. The restraint profiles obtained using this procedure are presented in Figures 16 and 17 for the walls tested at UoL and ICL, respectively. The restraint factor was greatest for the bottom row of demec points, adjacent to the joint

between the wall, and base and reduced fairly linearly with height above the base. There is no consistent variation in the measured restraint factors with time. In wall UoL-1, the restraint factor was greatest at early age and reduced with time with restraint profiles shifting almost uniformly to the left in Figure 16. This pattern was observed to a lesser extent in wall UoL-2 but not at all in wall ICL-2 where the base was older at the time of casting the wall (see Table 3) and cracking occurred.

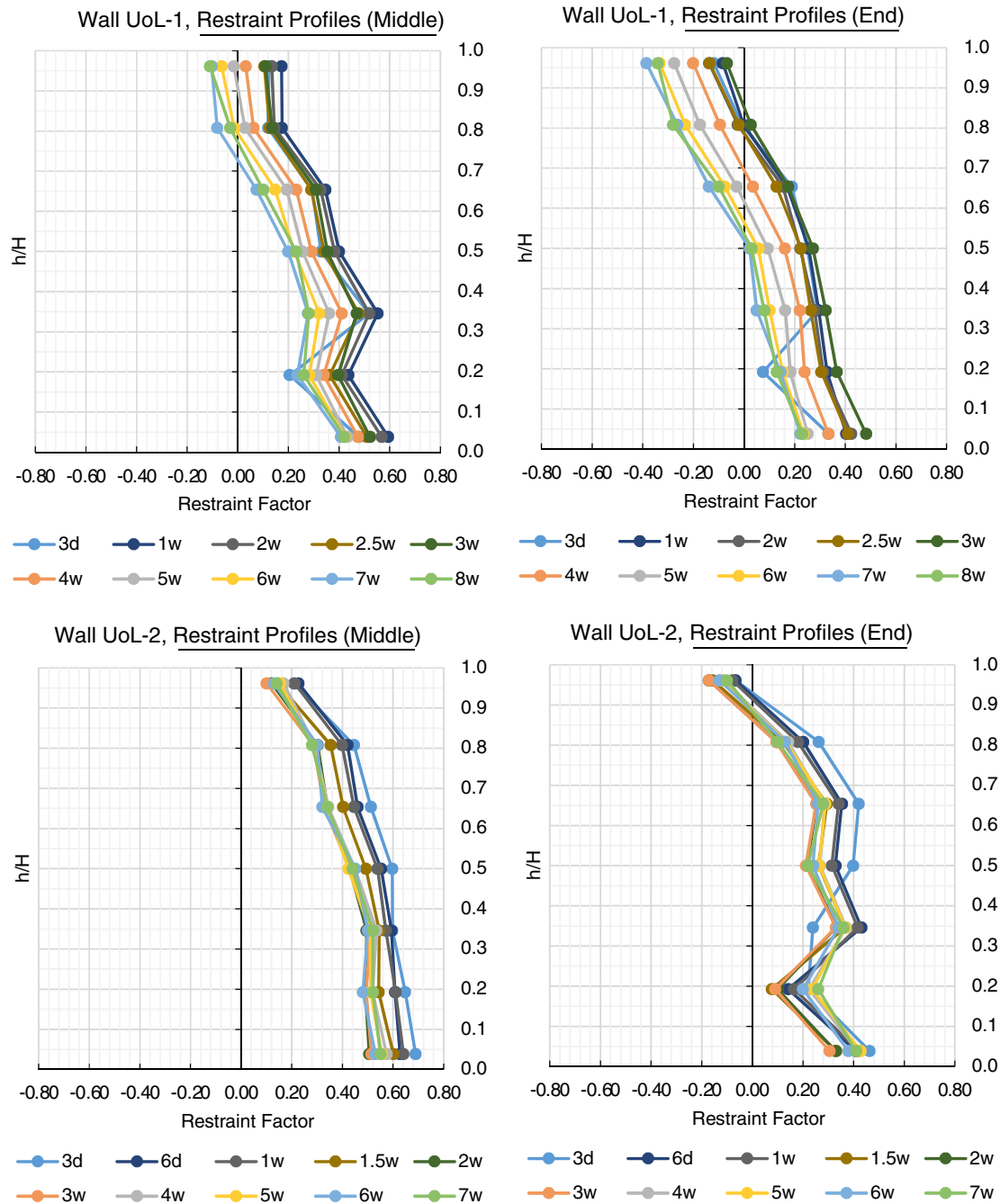


FIGURE 16 Restraint profiles at central and end parts of the walls at UoL. UoL, University of Leeds

Notably, the free shrinkage strain of concrete mix ICL-M2 used in wall ICL-2 was significantly greater than that of mix ICL-M1 used in the base of wall ICL-2. This is significant since, neglecting internal restraint from reinforcement, only differential free strain between the base and wall contributes to the restrained strain. If both the base and wall were to shorten equally the restraint factor would equal zero. The variation of restraint factor with time depends on the difference in free strain between the base and wall which in turn

depends on the peak temperature, concrete mix design, wall geometry and the age of the base at casting the wall.

For assessment of cracking risk in edge restrained members, C766¹⁰ uses Equations 2 and 3 below to calculate the restraint factor at a height above the base equal to 10% of the wall length.

$$R_j = \frac{1}{1 + \frac{A_{new} E_{new}}{A_{old} E_{old}}} \tag{2}$$

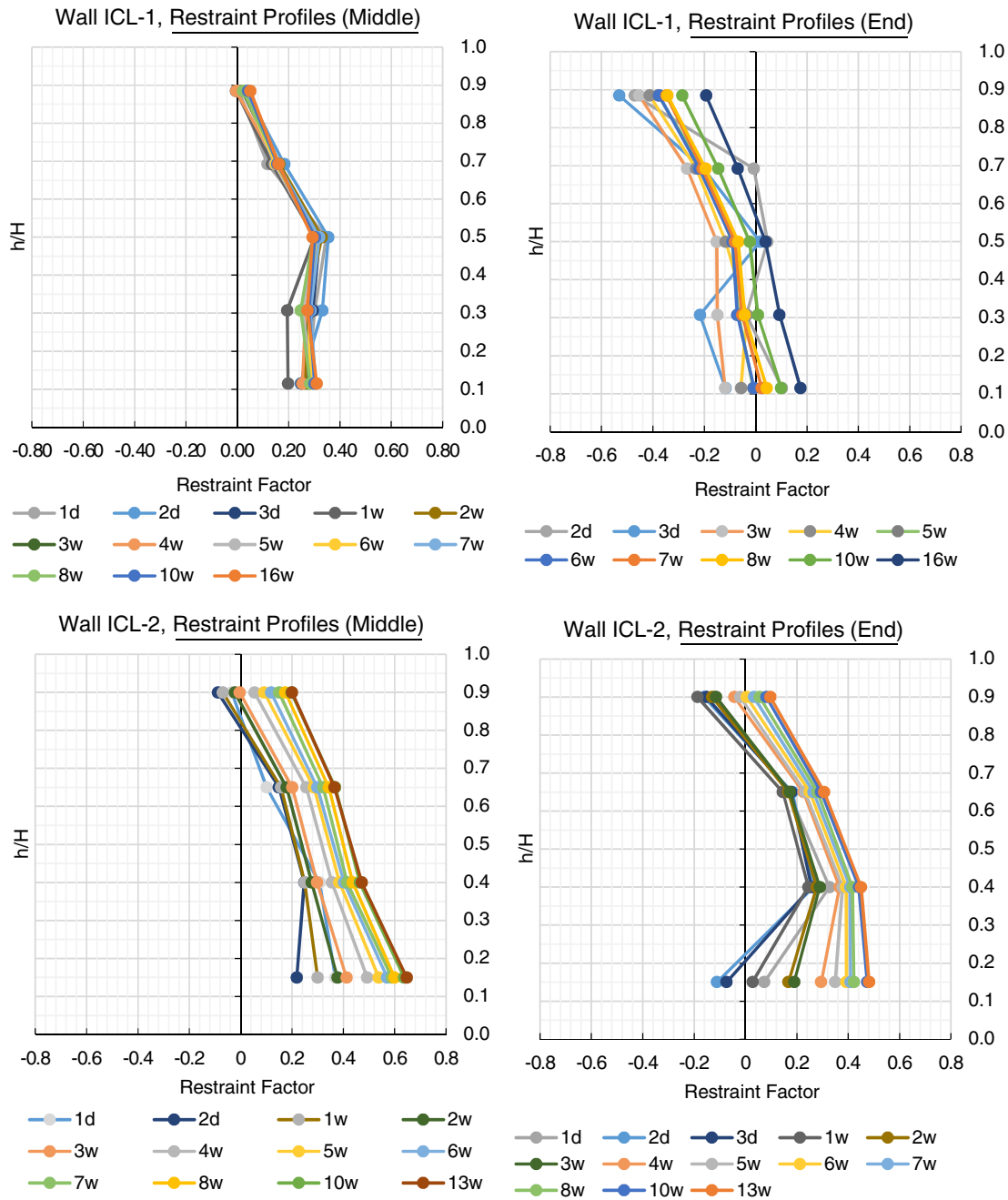


FIGURE 17 Restraint profiles at central and end parts of the walls at ICL. ICL, Imperial College London

in which R_j is the restraint factor at the joint, A_{new} and A_{old} are the cross-sectional areas of the new (restrained) element and the old (restraining) element. E_{new} and E_{old} are the moduli of elasticity for the new and old elements respectively. In absence of experimental data, C766¹⁰ suggests that the ratio $\frac{E_{new}}{E_{old}}$ is taken as 0.7 when calculating the restraint factor at 3 days (R_1) and as 1 when calculating the LT restraint factor, (R_2). Report C766 also gives the following equation to describe the variation of

restraint factor with height (h) in walls of height (H) and length (L):

$$R = R_j \left[\left(1.372(h/L)^2 - 2.543 \left(\frac{h}{L} \right) + 1 \right) + 0.044((L/H) - 1.969)(h/\times H)^{1.349} \right] \tag{3}$$

Report C766 allows for the effect of creep by reducing the calculated restraint factor by a multiple of 0.65 for early age free strain (3 days) and 0.5 for subsequent LT free

strain. Table 5 compares the measured restraint factors at a height of 0.1 L with those calculated using Equations 2 and 3 at 3 and 28 days. To account for creep, the calculated restraint factors were reduced by a multiple of 0.65 at 3 days and a composite value of 0.60 at 28 days. Table 5 shows that the measured restraint factors are greater than calculated once creep is accounted for as suggested in C766. Consequently, although the influence of creep relaxation on the restraint factors needs to be acknowledged and incorporated, the value of these creep coefficients should reflect relevant influencing factors such as mix proportions and environmental conditions. There is, therefore, a need to better define the value of these coefficients and perhaps optimize them to reflect the individual conditions.

2.5 | Prediction of cracking in edge restrained walls

The cracking risk is defined in C660⁷ and C766¹⁰ as the ratio of the restrained strain (ϵ_r) to the tensile strain capacity of the concrete (ϵ_{ctu}). A ratio $\epsilon_r/\epsilon_{ctu}$ of 1 or more is considered^{7,10} to indicate likely cracking. The ratio $\epsilon_r/\epsilon_{ctu}$ was calculated for the tested walls with the tensile strain capacity of concrete calculated using the following equation from C660⁷ which is based on field observations:

$$\epsilon_{ctu}(t) = 1.23 \left(0.63 + \frac{f_{cube}}{100} \right) f_{ctm}(t) / E_{cm}(t) \quad (4)$$

in which f_{cube} is the 28-day cube strength, $f_{ctm}(t)$ is the mean concrete tensile strength at time t and $E_{cm}(t)$ is the mean concrete elastic modulus at time t .

According to C660, the coefficient of 1.23 in Equation 4 accounts for creep as well as the reduction in failure stress under sustained load relative to the tensile strength under short-term loading. In evaluating Equation 4, f_{cube} was taken as the mean measured cube strength at 28 days. The ratio $f_{ctm}(t)/E_{cm}(t)$ was calculated at 28 days using measured material properties from Table 3 which were assumed to vary with time in accordance with the recommendations of EC2 for cement

strength class CEM 52.5 N. Figure 18 shows the variation with time of “cracking risk” defined^{7,10} as $\epsilon_r/\epsilon_{ctu}$. During the monitoring period, cracking only occurred in wall ICL-2 as suggested by Figure 18. Walls ICL-1 and UoL-2 appear to have been very close to cracking. Wall UoL-2 failed to crack, despite its large restraint factor, due to the relatively low peak temperature rise compared with ICL-2. It is also worth highlighting that in four similar tests previously carried out at UoL,^{2,6,25} the approach of Figure 18 was found to be accurate in predicting cracking and quite accurate in predicting the time of onset of cracking.

2.6 | Cracking description and width

Of the four walls tested in the work, only wall ICL-2 cracked due to restraint. The final crack pattern before loading in direct tension is shown for ICL-2 in Figure 19 which also gives measured final crack widths. Crack widths were measured on one side of the wall using a crack microscope with a measuring resolution of 0.02 mm. Cracking was monitored on the other side of the wall using DIC. The crack pattern and crack widths were similar on each side of the wall, but cracks developed independently in each face of the wall. Through cracks developed when the wall was externally loaded in direct tension as described in Section 1.2 but prior to this it was not possible through visual inspection alone to determine which cracks, if any, were through cracks. The maximum crack width recorded in the wall before loading was 0.1 mm. The first crack appeared in the middle zone of the wall, 11 days after it was cast, at around 245 mm above the base ($0.05L_{wall}$) and 60 mm to the left of the wall centreline. This first crack formed as a primary crack with a width of 0.08 mm. The second crack appeared 5 days later (day 16), at a height of 190 mm and at a distance of 590 mm to the right of the first crack. This second crack later formed part of a primary crack with a maximum width of 0.1 mm. Subsequent cracks appeared as short lengths in a random fashion but eventually connected to form longer cracks. The spacings between the adjacent well-defined longer cracks ranged between

TABLE 5 Comparison of experimentally derived and calculated restraint factors

Wall	At 3 days		At 28 days	
	Experimental	CIRIA C766	Experimental	CIRIA C766
ICL-1	0.31	0.27	0.27	0.21
ICL-2	0.21	0.30	0.32	0.24
UOL-1	0.46	0.27	0.37	0.21
UOL-2	0.60	0.34	0.50	0.28

140 to 210 mm. Maximum crack widths (w) were estimated, at a height of 10% of the wall length above the base as recommended in C766, in accordance with EC2 Part 3⁸ as a function of time as:

$$w = R\varepsilon_{\text{free}}S_{r,\text{max}} \tag{5}$$

in which R is the restraint factor, which was determined in accordance with Annex L of EC2 Part 3 and $S_{r,\text{max}}$ is the design crack spacing calculated in accordance with EC2¹⁸ which is 487 mm for wall ICL-2. The restraint factor at a height of 10% of the wall length above the base was determined by linearly interpolating between the restraint factors given in Table L1 of EC2 Part 3 for the top and bottom of the wall. The strain $\varepsilon_{\text{free}}$ was calculated at the same position in terms of the measured peak temperature drop.

Figure 20 compares the measured and predicted development of maximum crack width with time. The comparison between measured and predicted crack widths is reasonable despite both the measured crack spacing and restrained strain being less than calculated with EC2. This is surprising since calculating the maximum crack width as the product of the experimentally determined crack inducing strain and the EC2 design crack spacing of 487 mm should theoretically lead to the crack width being overestimated by a multiple of $487/210 = 2.3$. It is also interesting to note that the maximum crack width remained fairly constant between 14 and 70 days despite the increase in restrained strain during this time. Consequently, it appears that the relationship between restrained strain and crack width requires further investigation.

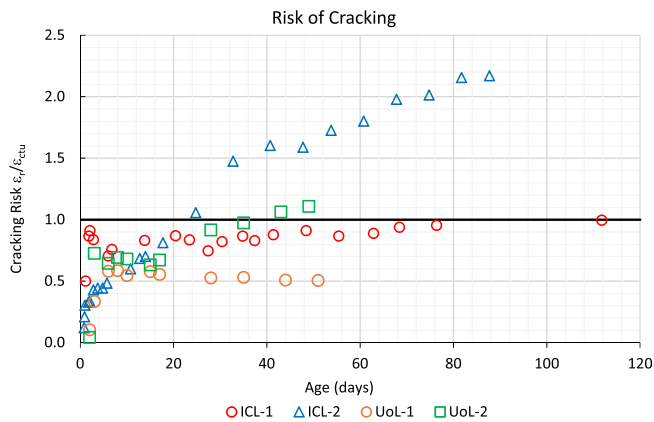


FIGURE 18 Risk of cracking

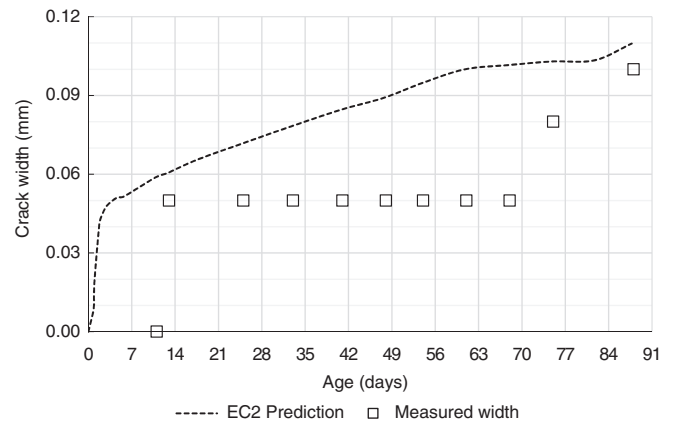


FIGURE 20 Comparison of measured and predicted crack width for wall ICL-2. ICL, Imperial College London

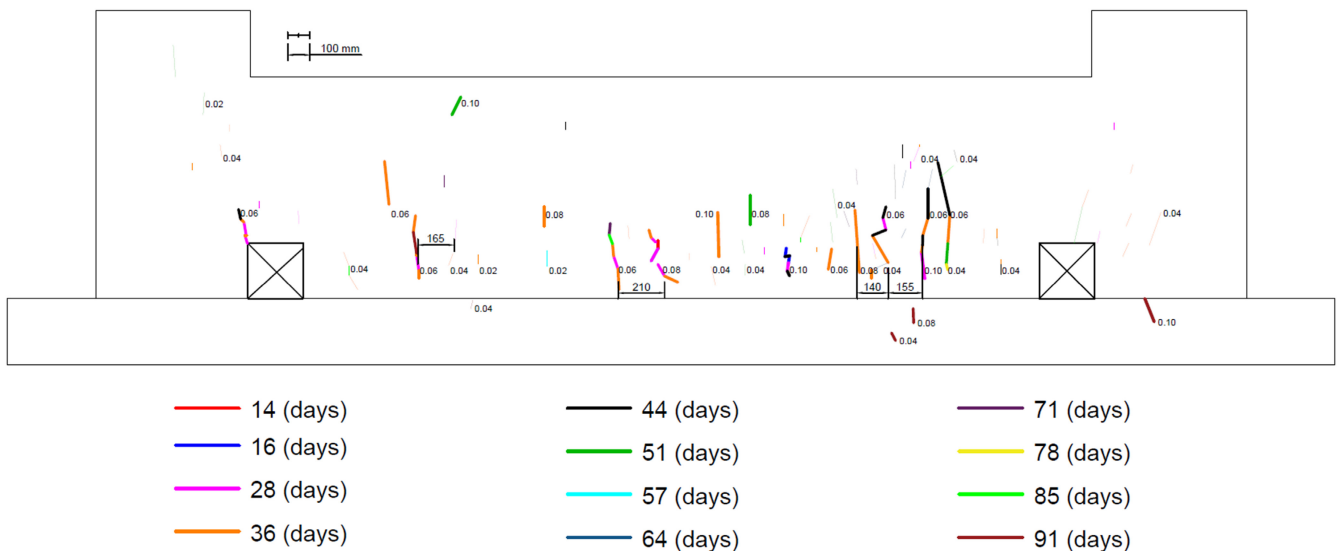


FIGURE 19 Crack layout and width for wall ICL-2. ICL, Imperial College London

3 | CONCLUSION

The results of four tests conducted at ICL and the UoL to investigate the behavior of edge restrained walls are presented in this paper. Selection of suitable formwork and thermal insulation was found to be essential if magnification of the imposed strains is desired for experimental investigations in laboratories. The early age temperature profile in the walls was found to be significantly affected by heat flow into the base. The effect of this is beneficial since it reduces the restrained strain near the bottom of the wall where restraint is greatest. CIRIA report C660 predicts cracking to occur if the ratio of the restrained strain (ϵ_r) to the tensile strain capacity of concrete (ϵ_{ctu}) exceeds 1. The maximum value of $\epsilon_r/\epsilon_{ctu}$ was calculated for each wall and was only significantly greater than 1 for wall ICL-2 which was the only wall to crack. Similarly, Shehzad⁶ only observed cracking in walls where $\epsilon_r/\epsilon_{ctu}$ calculated in accordance with C660 exceeded 1. Crack widths in wall ICL-2 were reasonably predicted by EC2.

ACKNOWLEDGMENTS

The authors kindly acknowledge financial support from the Engineering and Physical Sciences Research Council (EPSRC) under grants EP/T004142/1 and EP/T004185/1 titled "understanding the cracking behavior of reinforced concrete elements subjected to the restraint of imposed strains."

DATA AVAILABILITY STATEMENT

The data that support the findings of this study are available from the corresponding author upon reasonable request.

ORCID

Muhammad Shehzad  <https://orcid.org/0000-0002-2078-7651>

Robert Vollum  <https://orcid.org/0000-0003-1075-2014>

John Forth  <https://orcid.org/0000-0002-4594-1475>

Nikolaos Nikitas  <https://orcid.org/0000-0002-6243-052X>

REFERENCES

- Jędrzejewska A, Kanavaris F, Zych M, Schlicke D, Azenha M. Experiences on early age cracking of wall-on-slab concrete structures. *Structures*. 2020;27:2520–49.
- Shehzad MK, Forth JP, Bradshaw A. Imposed loading effects on reinforced concrete walls restrained at their base. *Proc Inst Civil Eng Struct Build*. 2020;173(6):413–28.
- Stoffers H. Cracking due to shrinkage and temperature variation in walls. *HERON*. 1978;23(3):63.
- Kheder GF, Al Rawi S, Al Dhahi JK. Study of the behavior of volume change cracking in base restraint concrete walls. *ACI Mater J*. 1994;91:150–7.
- Micallef M, Vollum RL, Izzuddin BA. Crack development in transverse loaded base-restrained reinforced concrete walls. *Eng Struct*. 2017;143:522–39.
- Shehzad MK. Influence of vertical steel reinforcement on the behaviour of edge restrained reinforced concrete walls [PhD thesis]. Leeds, UK: University of Leeds; 2018.
- Bamforth P. Early-age thermal crack control in concrete. London: CIRIA C660; 2007.
- BSI. BS EN 1992–3 Eurocode 2: Design of Concrete Structures. Part 3: Liquid retaining and containment structures. London UK: BSI; 2006.
- fib. fib Model Code for Concrete Structures 2010. Berlin, Germany: Ernst & Sohn; 2013.
- Bamforth P. Control of cracking caused by restrained deformation in concrete. London: CIRIA C766; 2018.
- Kanavaris F, Kaethner S. CIRIA guide C766: an overview of the updated CIRIA C660 guidance on control of cracking in reinforced concrete structures. Paper presented at: International RILEM Conference on Sustainable Materials, Systems and Structures—SMSS192019.
- Saeed MK, Rahman MK, Baluch MH, Tooti LA. Cracking in concrete water tank due to restrained shrinkage and heat of hydration: field investigations and 3D finite element simulation. *J Perform Constr Facil*. 2020;34(1):04019100.
- Seruga A, Zych M. Thermal cracking of the cylindrical tank under construction. I: Case study. *J Perform Constr Facil*. 2015; 29(4):04014100.
- BSI. BS EN 12390-3 Testing hardened concrete. Part 3: Compressive strength of test specimens. London, UK: BSI; 2019.
- BSI. BS EN 12390-6 Testing hardened concrete. Tensile splitting strength of test specimens. London, UK: BSI; 2010.
- BSI. BS EN 12390–13:2013. Part 13: Determination of secant modulus of elasticity in compression. London, UK: BSI; 2013.
- CEN/TC 250/SC 2. prEN1992-1-1:2021-09 Eurocode 2: Design of concrete structures - Part 1-1: General rules - Rules for buildings, bridges and civil engineering structures. Brussels; CEN-CENLAC; 2021.p. 375.
- BSI. BS EN 1992-1-1: Eurocode 2: Design of Concrete Structures: Part 1-1: General Rules and Rules for Buildings. London, UK: BSI; 2004.
- Neville A, Adam M. Properties of concrete. England: Prentice Hall; 2002.
- Gribniak V, Torres L, Kaklauskas G, Daniunas A, Kacianauskas R, Jakubovskis R. Prediction of concrete shrinkage occurring prior to external loading and effect on short-term constitutive modeling and design. *Adv Struct Eng*. 2013;16(6):1061–80.
- ACI Committee 209 Guide for modeling and calculating shrinkage and creep in hardened concrete. ACI Committee 209 report. 2008;209.
- CNIS (Central Institute of Research and Investigation in Civil Engineering). Recommendations for Determination of Numerical Parameters of Creep and Shrinkage of Concrete for Design of Reinforced Concrete Structures in the Regions of Dry and Hot Climate, CNIIS, Moscow, Russia. 1983 (in Russian).
- Bazant ZP, Baweja S. Justification and refinements of model B3 for concrete creep and shrinkage part 1. Statistics and sensitivity. *Mater Struct*. 1995;28(7):415–30.
- Gardner N, Lockman M. Design provisions for drying shrinkage and creep of normal-strength concrete. *Mater J*. 2001;98(2):159–67.
- Shehzad MK, Forth JP, Bradshaw A. Imposed loading effects on reinforced concrete walls restrained at their base. *Proceedings of the Institution of Civil Engineers-structures and buildings*; London: Tomas Telford; 2019. p. 1–17.

AUTHOR BIOGRAPHIES



Abobakr Elwakeel, Department of Civil and Environmental Engineering, Imperial College London, London, UK.
a.elwakeel15@imperial.ac.uk



Muhammad Shehzad, School of Civil Engineering, University of Leeds, Leeds, UK.
m.k.shehzad@leeds.ac.uk



Karim El Khoury, Department of Civil and Environmental Engineering, Imperial College London, London, UK.
k.khoury20@imperial.ac.uk



Robert Vollum, Department of Civil and Environmental Engineering, Imperial College London, London, UK.
r.vollum@imperial.ac.uk



John Forth, School of Civil Engineering, University of Leeds, Leeds, UK.
j.p.forth@leeds.ac.uk



Bassam Izzuddin, Department of Civil and Environmental Engineering, Imperial College London, London, UK.
b.izzuddin@imperial.ac.uk



Nikolaos Nikitas, School of Civil Engineering, University of Leeds, Leeds, UK.
n.nikitas@leeds.ac.uk

How to cite this article: Elwakeel A, Shehzad M, El Khoury K, Vollum R, Forth J, Izzuddin B, et al. Assessment of cracking performance in edge restrained RC walls. *Structural Concrete*. 2022;23: 1333–52. <https://doi.org/10.1002/suco.202100688>